Adsorption of Selenium and Strontium on Goethite: EXAFS Study and Surface Complexation Modeling of the Ternary Systems

Zhe Nie,[†,‡] Nicolas Finck,[‡] Frank Heberling,[*,‡] Tim Pruessmann,[§,∥] Chunli Liu,[*,†] and Johannes Lützenkirchen[‡]

[†]Beijing National Laboratory for Molecular Sciences, Fundamental Science Laboratory on Radiochemistry and Radiation Chemistry, College of Chemistry and Molecular Engineering, Peking University, Beijing, 100871, China

[‡]Institute for Nuclear Waste Disposal, Karlsruhe Institute of Technology, Hermann von Helmholtz Platz 1, 76344 Eggenstein Leopoldshafen, Germany

[§]Institute of Catalysis Research and Technology, Karlsruhe Institute of Technology, Hermann von Helmholtz Platz 1, 76344 Eggenstein Leopoldshafen, Germany

[∥]Institute for Chemical Technology and Polymer Chemistry, Karlsruhe Institute of Technology, Engesserstr. 20, 76131 Karlsruhe, Germany

ABSTRACT: Knowledge of the geochemical behavior of selenium and strontium is critical for the safe disposal of radioactive wastes. Goethite, as one of the most thermody namically stable and commonly occurring natural iron oxy hydroxides, promisingly retains these elements. This work comprehensively studies the adsorption of Se(IV) and Sr(II) on goethite. Starting from electrokinetic measurements, the binary and ternary adsorption systems are investigated and systematically compared via batch experiments, EXAFS analysis, and CD MUSIC modeling. Se(IV) forms bidentate inner sphere surface complexes, while Sr(II) is assumed to form outer sphere complexes at low and intermediate pH and inner sphere complexes at high pH. Instead of a direct interaction between Se(IV) and Sr(II), our results indicate an electrostatically driven mutual enhancement of adsorption. Adsorption of Sr(II) is promoted by an average factor of 5 within the typical groundwater pH range from 6 to 8 for the concentration range studied here. However, the interaction between Se(IV) and Sr(II) at the surface is two sided, Se(IV) promotes Sr(II) outer sphere adsorption, but competes for inner sphere adsorption sites at high pH. The complexity of surfaces is highlighted by the inability of adsorption models to predict isoelectric points without additional constraints.
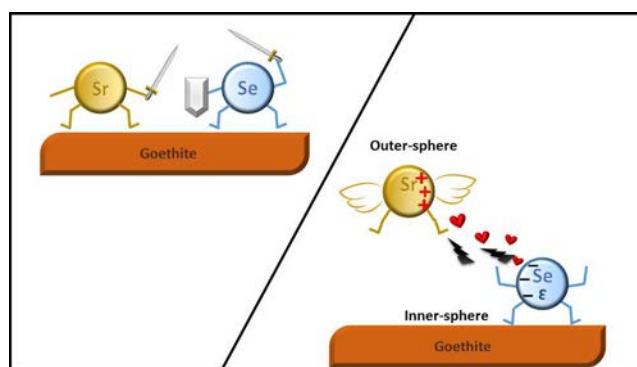
1. INTRODUCTION

As numerous countries exploit nuclear energy, critical environ mental issues arise from the treatment and disposal of the hazardous spent fuel and related radioactive wastes. Significant contributions to the total dose of radioactive wastes originate from ^{90}Sr ($T_{1/2}$ = 28.9 a) and ^{79}Se ($T_{1/2}$ = 2.95 × 10^5 a), and will last during the first one hundred years[1] and the next million years,[2] respectively. Because of the high solubility and the long half life, ^{79}Se is recognized as one of the key radionuclides in performance assessment for high level radioactive waste (HLW) repositories.[3] The relevance of strontium originates from the high concentration of ^{90}Sr in radioactive waste and contaminations associated with nuclear accidents.[4] Besides, both elements are bioavailable: selenium is a well known essential micronutrient for humans and animals[5] and strontium can accumulate in the hydroxyapatite of teeth and bones.[6] With respect to the potential leakage from a HLW repository, the prospective backfill clay materials show only limited ability to immobilize the highly soluble selenium and strontium species.[1] In contrast, iron oxides and iron oxy hydroxides, both ubiquitous in surface and subsurface environments and as common corrosion products of steel containers for HLW[7] at oxidizing conditions, are good sorbents for metal cations. They are used for environmental remediation purposes.[8,9] Thus, strong environmental and geochemical efforts are undertaken to investigate the immobilization and speciation of Sr(II) and Se(IV) at iron oxide and iron oxy hydroxide surfaces.

Goethite (α FeOOH) is one of the most thermodynamically stable and commonly occurring natural iron oxy hydroxides.[10]

It shows an acicular morphology with the (110) face being the dominant crystallographic surface plane.[11] Over the years, various sites at the goethite surface have been invoked to interpret sorption data.[12−16] Infrared spectroscopy data indicate the presence of three different surface hydroxyl groups, which are singly ($\equiv$FeOH$^{-1/2}$), doubly ($\equiv$Fe$_2$OH), and triply ($\equiv$Fe$_3$O$^{-1/2}$) coordinated.[17] Usually two kinds of surface groups are considered, singly ($\equiv$FeOH$^{-1/2}$) and triply ($\equiv$Fe$_3$O$^{-1/2}$) coordinated groups,[18−21] because the doubly ($\equiv$Fe$_2$OH) coordinated group is both uncharged and unreactive toward protonation, deprotonation, and ion binding in the pH range 2−12.[13,22]

Previous extended X ray absorption fine structure (EXAFS) spectroscopy studies have shown that Se(IV) strongly binds to the goethite surface involving two singly coordinated hydroxyl groups, forming an inner sphere surface complex.[23] A charge distribution multisite complexation (CD MUSIC) model for Se(IV) adsorption on goethite has been established by fitting sorption envelope data.[19] It shows that the dominant species is $\equiv$(FeO)$_2$SeO, in agreement with EXAFS spectroscopy. As for strontium, EXAFS data indicate outer sphere surface complexes with goethite at moderate pH[24] and inner sphere complexes at alkaline conditions.[24,25] Accordingly, a modeling exercise on Sr(II) adsorption at goethite at pH 6−10 applies only outer sphere species.[26]

The adsorption of cations may be significantly influenced by the presence of anions, and vice versa.[21,27,28] This is especially true for anionic species strongly binding to mineral surfaces, such as phosphate and selenite. To our knowledge, studies focused on the coadsorption of Sr(II) and Se(IV) have not been published before. Investigations in the ternary system including the structural analysis of potential ternary species are of particular interest. For such studies, it is necessary to investigate Sr(II) and Se(IV) adsorption at high surface loadings, which may exceed natural concentration levels. However, considering the chemical similarity of Se(IV) and Sr(II) to environmentally ubiquitous carbonate and Ca(II), effects observed in the ternary Se(IV)−Sr(II)−goethite system may be comparable to phenomena occurring in the presence of these naturally more abundant ions.

Our work intends to provide missing information by investigating the ternary system, exploring the mutual effects of Sr(II) and Se(IV) adsorption on goethite. The uptake of Sr(II) and Se(IV) by goethite is examined in binary systems and in the ternary system. Starting from electrokinetic measurements and batch sorption experiments, we study the electrophoretic mobility and solute uptake as a function of pH, ion concentration, and addition order. EXAFS spectroscopy is used to probe the molecular scale environment of adsorbed Sr and Se species. Finally, CD MUSIC models are developed and compared to experimental data, and detailed information on surface speciation and the synergistic adsorption effects is derived.

2. MATERIALS AND METHODS

2.1. Materials and Chemicals. The goethite is prepared as in previous studies.[13,14] The acicular shape and the purity are assessed by SEM (Quanta 650 FEG, FEI) and XRD (D8 Advance, Bruker) (cf. Supporting Information Figure S1). The specific surface area, measured by BET N$_2$ adsorption (AUTOSORB 1, Quantachrom Corporation), is 98 m^2/g. Stock solutions of 0.1 M Se(IV) and 1 M Sr(II) are prepared from Na$_2$SeO$_3$(s) (Sigma Aldrich) and SrCl$_2$·6H$_2$O(s)

(Merck). All other chemicals used in this study are A.R. grade. All solutions and suspensions are prepared by weight, diluted with ultrapure water (18.2 MΩ·cm, Milli Q system, Millipore), and adjusted to the desired pH by adding small volumes of HCl or NaOH solutions.

2.2. Adsorption Experiments and Electrokinetic Measurements. In the initial phase of the adsorption experiments, suspensions are prepared for the electrokinetic measurements to probe particle electrokinetics. The so called zeta potential refers to the electrostatic potential at the slipping plane. It is, however, an ambiguous measure. From theoretical perspective, the exact position of the slipping plane is unknown and the diffuse layer potential at the head end of the diffuse layer is not necessarily equal to zeta potential. With respect to experimental measurement, zeta potential is calculated from the measured electrophoretic mobility assuming a spherical particle geometry. Such calculations may lead to wrong results for the needle shaped goethite particles. Nevertheless, the point of zero electrophoretic mobility and zero diffuse layer potential, i.e. the isoelectric point (IEP), is unambiguous and enables us to compare the experimental data and model results. Thus, to avoid those uncertainties, we focus on the unambiguous IEP for model development and report only electrophoretic mobilities, μ ((μm/s)/(V/cm)), as the characteristic measured quantity for the particle diffuse layer potential. Phase analysis light scattering (PALS) measurements are used to determine electrophoretic mobility using a "ZetaPlus" zeta potential analyzer (Brookhaven Instruments Co.). First, the electro phoretic mobility of goethite particles is determined as a function of pH and Se(IV) concentration. Samples are prepared as 1 g/L goethite suspension containing 0, 0.1, 0.25, or 1 mM Se(IV), and adjusted to the desired pH value. Electrophoretic mobilities are recorded after overnight equilibration. Second, the influences of type and concentration of cations on the electrokinetics are investigated. Goethite suspensions (1 g/L) in contact with Se(IV) (0, 0.25, or 1 mM) are prepared at pH 6.0 or 10.5. Afterward, an aliquot of LiCl, NaCl, CsCl, CaCl$_2$, or SrCl$_2$ stock solution is added to reach final cation concentrations of 0, 0.002, 0.01, 0.05, 0.1, and 0.2 M, respectively. The binary samples (cation + goethite) are adjusted to pH 10.5, while ternary samples (cation + selenite + goethite) are adjusted to pH 6.0 in order to have a comparable starting electrophoretic mobility of −1 (μm/s)/ (V/cm) (dashed line in Figure 1) before starting with cation addition. Third, the effect of addition order is examined with 1 g/L goethite suspensions, 0.25 mM Se(IV) and Sr(II) at pH 6 and 10.5. A time interval of 12 h is allowed before addition of the third component.

In a next step, sorption envelopes and pH edges are measured for the binary (goethite + Se(IV) or goethite + Sr(II)) and ternary (goethite + Se(IV) + Sr(II)) systems. Suspensions containing 1 g/L goethite, 0.25 mM adsorbates in 10 mM NaCl are prepared, adjusted to the desired pH, equilibrated, and subjected to both ICP MS analysis and electrokinetic measurements. The adsorbed amount is calcu lated from the difference between the initial and the final aqueous concentrations. Solid−liquid separation is performed with 1 h ultracentrifugation at 90 000 rpm. ICP MS analyses are performed on an XSeries 2 (Thermo Scientific).

During sample preparation, great care is taken to avoid contact of the suspensions with CO$_2$ by flushing solutions and suspensions with Ar. Goethite suspensions for each exper imental series are freshly prepared from a stock suspension.
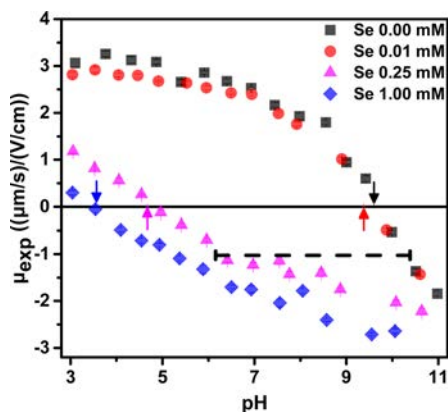
Figure 1. Electrophoretic mobility (μ_{exp}) of goethite suspensions as a function of Se(IV) loading and pH. Arrows show the IEPs calculated by the model, and dashed line shows the equivalent starting mobility for cation adsorption experiments.

2.3. EXAFS Spectroscopy. Adsorption samples containing 1 g/L goethite, 10 mM NaCl, and 0.25 mM adsorbate with different addition orders at pH 6 and 10.5 are freshly prepared for EXAFS analysis. After equilibration, the solid part is separated, washed with ethanol, and dried in an Ar glovebox. Samples are measured in an airtight PEEK sample holder with a Kapton window. Dry powder is introduced into the sample holder just prior to analysis and the internal space of the sample holder is flushed with helium for half an hour. This procedure efficiently prevents oxidation of Se(IV) under the beam.

XAS spectra are collected at the ACT experimental station of the CAT ACT beamline[29] at the Ångstroem Quelle Karlsruhe (ANKA). Beam energy is calibrated using a Pb foil (Pb L_1 edge at 15861 eV) for Sr measurements (Sr K edge 16105 eV), and a Se foil for Se measurement (Se K edge at 12658 eV). XAS data

are recorded in fluorescence mode at room temperature using a silicon drift detector (Vortex ME4, Hitachi).

For each sample, 6−8 scans are collected to achieve an adequate signal to noise ratio. Data reduction and modeling of the EXAFS spectra are performed using Athena (v. 0.9.24) and Artemis (v. 0.9.24) interfaces to the IFEFFIT software.[30] Plausible adsorption structures, based on the goethite (110) face structure and bond distances inferred from preliminary EXAFS fits, are constructed using the Diamond software (v.3.1) and the coordinates of atoms are imported to FEFF7[31] to calculate theoretical backscattering amplitude and phase shift functions. Coordination number (N), energy shift (ΔE_0), adjustment to interatomic distance (ΔR), and the Debye−Waller parameter (σ^2) are treated as fitting parameters for each shell, while the amplitude reduction factor (S_0^2) is set according to literature values.[23,32,33] Models are adjusted shell by shell to the Fourier transform of the k^2 and k^3 weighted spectra.

2.5. CD-MUSIC Modeling. In this work, a three plane CD MUSIC model is employed to describe the adsorption data and to simulate isoelectric points. Concerning electrostatic proper ties, the model is developed to reproduce isoelectric points (IEP, points of zero electrophoretic mobility). Due to the ambiguities mentioned above we do not attempt to quantitatively reproduce zeta potentials. Goethite surfaces were studied in great detail by Hiemstra, van Riemsdijk, and co workers.[12,13,19,21] Thus, our models are adapted from their work while adding Sr(II) and Se(IV) surface species. Three surface groups, i.e. $\equiv$FeOH$^{-1/2}$, $\equiv$Fe$_3$O$_I^{-1/2}$ and $\equiv$Fe$_3$O$_{II}^{-1/2}$, the respective site densities, and proton affinities in Table 1 are taken from Hiemstra et al.[12] or for a simplified model from Rahnemaie et al.[21](cf. SI Table S1). Some detailed discussion on model variants tested can be found in the SI. The aqueous speciation scheme is given in SI Table S2. The binding fashions of Se(IV) and Sr(II) in the model are deduced from our

Table 1. Parameters for the Surface Species in the Best Fit Model[a]

surface species	Δz_0	Δz_1	Δz_2	reaction	log K
$\equiv$FeOH$^{-1/2}$	0	0	0		0
$\equiv$FeOH$_2^{+1/2}$	1^c	0	0	$\equiv$FeOH$^{-1/2}$ + H$^+$ $\leftrightarrow$ $\equiv$FeOH$_2^{+1/2}$	7.7^b
$\equiv$FeOH$^{-1/2}$ Na$^+$	0	1^c	0	$\equiv$FeOH$^{1/2}$ + Na$^+$ $\leftrightarrow$ $\equiv$FeOH$^{-1/2}$ Na$^+$	0.61^c
$\equiv$FeOH$_2^{+1/2}$ Cl$^-$	0	1^c	0	$\equiv$FeOH$_2^{+1/2}$ + Cl$^-$ $\leftrightarrow$ $\equiv$FeOH$_2^{+1/2}$ Cl$^-$	0.44^c
$\equiv$Fe$_3$O$_I^{-1/2}$	0	0	0		0
$\equiv$Fe$_3$O$_I$H$^{+1/2}$	1	0	0	$\equiv$Fe$_3$O$_I^{-1/2}$ + H$^+$ $\leftrightarrow$ $\equiv$Fe$_3$O$_I$H$^{+1/2}$	11.7^b
$\equiv$Fe$_3$O$_I^{-1/2}$ Na$^+$	0	1^c	0	$\equiv$Fe$_3$O$_I^{-1/2}$ + Na$^+$ $\leftrightarrow$ $\equiv$Fe$_3$O$_I^{-1/2}$ Na$^+$	0.61^c
$\equiv$Fe$_3$O$_I$H$^{+1/2}$ Cl$^-$	0	1^c	0	$\equiv$Fe$_3$O$_I$H$^{+1/2}$+ Cl$^-$ $\leftrightarrow$ $\equiv$Fe$_3$O$_I$H$^{+1/2}$ Cl$^-$	0.44^c
$\equiv$Fe$_3$O$_{II}^{-1/2}$	0	0	0	-	0
$\equiv$Fe$_3$O$_{II}$H$^{+1/2}$	1^c	0	0	$\equiv$Fe$_3$O$_{II}^{-1/2}$ + H$^+$ $\leftrightarrow$ $\equiv$Fe$_3$O$_{II}$H$^{+1/2}$	0.2^b
$\equiv$Fe$_3$O$_{II}^{-1/2}$ Na$^+$	0	1^c	0	$\equiv$Fe$_3$O$_{II}^{-1/2}$ + Na$^+$ $\leftrightarrow$ $\equiv$Fe$_3$O$_{II}^{-1/2}$ Na$^+$	0.61^c
$\equiv$Fe$_3$O$_{II}$H$^{+1/2}$ Cl$^-$	0	1^c	0	$\equiv$Fe$_3$O$_{II}$H$^{+1/2}$+ Cl$^-$ $\leftrightarrow$ $\equiv$Fe$_3$O$_{II}$H$^{+1/2}$ Cl$^-$	0.44^c
$\equiv$(FeO)$_2$SeO$^-$	1.05^d	1.05^d	0	2$\equiv$FeOH$^{-1/2}$ + H$_2$SeO$_3$ $\leftrightarrow$ $\equiv$(FeO)$_2$SeO$^-$ + H$_2$O	14.31^d
$\equiv$(FeOH)$_2$Sr$^+$	2^d	0	0	2$\equiv$FeOH$^{-1/2}$ + Sr^{2+} $\leftrightarrow$ $\equiv$(FeOH)$_2$Sr$^+$	3.21^d
$\equiv$(FeOH)$_2$Sr$^+$ Cl$^-$	0	0	1^d	$\equiv$(FeOH)$_2$Sr$^+$ + Cl$^-$ $\leftrightarrow$ $\equiv$(FeOH)$_2$Sr$^+$ Cl$^-$	2.15^d
$\equiv$FeOH$^{-1/2}$ Sr^{2+}	0	2^d	0	$\equiv$FeOH$^{-1/2}$ + Sr^{2+} $\leftrightarrow$ $\equiv$FeOH$^{-1/2}$ Sr^{2+}	3.50^d
$\equiv$FeOH$^{-1/2}$ Sr^{2+} Cl$^-$	0	0	1^d	$\equiv$FeOH$^{-1/2}$ Sr^{2+} + Cl$^-$ $\leftrightarrow$ $\equiv$FeOH$^{-1/2}$ Sr^{2+} Cl$^-$	2.15^d
$\equiv$Fe$_3$O$_I^{-1/2}$ Sr^{2+}	0	2^d	0	$\equiv$Fe$_3$O$_I^{-1/2}$ + Sr^{2+} $\leftrightarrow$ $\equiv$Fe$_3$O$_I^{-1/2}$ Sr^{2+}	3.50^d
$\equiv$Fe$_3$O$_I^{-1/2}$ Sr^{2+} Cl$^-$	0	0	1^d	$\equiv$Fe$_3$O$_I^{-1/2}$ Sr^{2+} + Cl$^-$ $\leftrightarrow$ $\equiv$Fe$_3$O$_I^{-1/2}$ Sr^{2+} Cl$^-$	2.15^d
$\equiv$Fe$_3$O$_{II}^{-1/2}$ Sr^{2+}	0	2^d	0	$\equiv$Fe$_3$O$_{II}^{-1/2}$ + Sr^{2+} $\leftrightarrow$ $\equiv$Fe$_3$O$_{II}^{-1/2}$ Sr^{2+}	3.50^d
$\equiv$Fe$_3$O$_{II}^{-1/2}$ Sr^{2+} Cl$^-$	0	0	1^d	$\equiv$Fe$_3$O$_{II}^{-1/2}$ Sr^{2+} + Cl$^-$ $\leftrightarrow$ $\equiv$Fe$_3$O$_{II}^{-1/2}$ Sr^{2+} Cl$^-$	2.15^d

$^a\Delta z_0$, Δz_1, and Δz_2 represent the change of charge at 0 , 1 , and 2 planes, respectively. In the model it is assumed that the (110) plane is dominating. Log K is calculated on a mole fraction scale. The capacitances are C$_1$ = C$_2$ = 0.92 F/m^2. Site densities for $\equiv$FeOH$^{-1/2}$, $\equiv$Fe$_3$O$_I^{-1/2}$, and $\equiv$Fe$_3$O$_{II}^{-1/2}$ are set to 3, 6, and 3 nm^{-2}, respectively. ^{b}From Hiemstra et al.[12] ^{c}From Rahnemaie et al.[21] ^{d}Determined in this work.
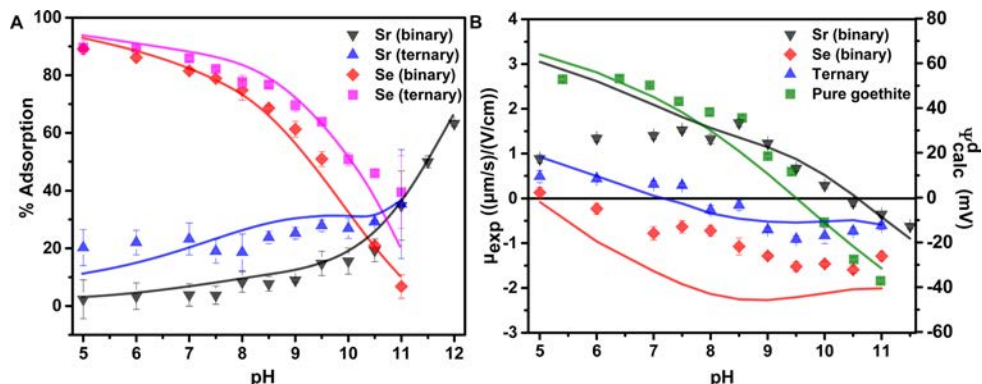
Figure 2. Solute uptake (A) and electrophoretic mobility (B) at 0.25 mM Sr(II) and Se(IV) in 10 mM NaCl as a function of pH. Points represent measured data. Curves plotted on the right y axis depict the diffuse layer potential predicted by the model (Table 1).
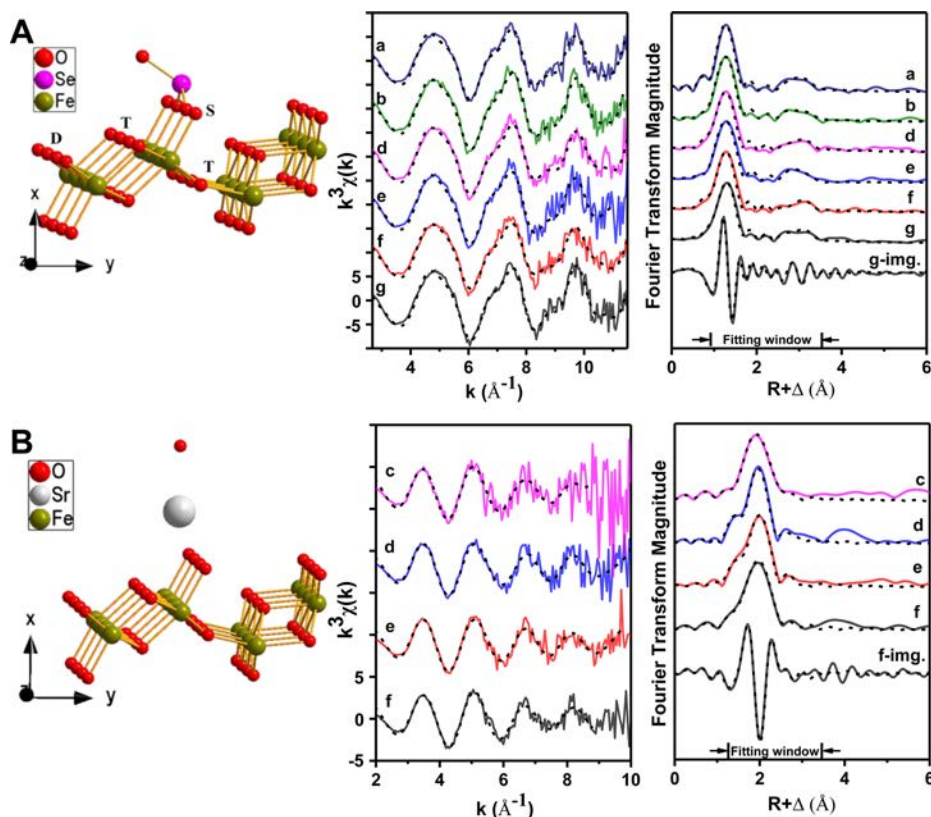
Figure 3. Structures assumed in FEFF calculations (left), EXAFS spectra in k space (middle), and corresponding Fourier transforms (right) for selenium (A) and strontium (B). "S", "D", and "T" denote singly, doubly, and triply coordinated surface oxygen atoms, respectively. The sample coding is specified in Tables 2 and 3. The single oxygen atom above Sr in the left image in 3B represents hydration water molecules. Exemplarily, the imaginary parts of the curves A−g and B−f are shown. Solid lines represent data; the model curves are shown as dashed lines.

EXAFS results and from literature results.[24,25] Corresponding equilibrium constants are optimized through least squares fitting. The models are developed step by step, from the adjustment to fit adsorption data to the inclusion of electrokinetic information. Model development is performed using a modified version of FITEQL[34] coupled to UCODE.[35]

3. RESULTS AND DISCUSSION

3.1. Electrokinetic Information. The particle interfacial electrostatic potential is illustrated by electrophoretic mobility (Figure 1). The well known zeta potential or the potential at diffuse layer is proportional to electrophoretic mobility. For pure goethite samples, the mobility becomes increasingly positive as the pH decreases, indicating protonation of surface functional groups. We find the isoelectric point (IEP) of pure goethite at pH 9.7, somewhat higher than in previous studies on comparable preparations.[18,19] High IEP indicates the absence of CO_2 and predominance of the (110) face.[20] When 0.01 mM Se(IV) is added to the goethite suspensions, the IEP shifts to a slightly lower value. With higher Se(IV) concentrations (0.25 mM and 1 mM), the IEP significantly shifts to lower pH values. The IEP shift can be regarded as a good qualitative indicator of anion adsorption in particular at high surface loading when Se(IV) concentration is above 0.25 mM. The IEPs can be well described by the proposed model (model IEPs are indicated by arrows in Figure 1).

Table 2. Best Fit EXAFS Model Parameters for Selenium Adsorbed on Goethite

coding	sample[a]	pH	ΔE_0 (eV)	N[b]	path Se O[c] R (Å)	path Se O[c] σ^2 (Å²)	path Se Fe[c] N	path Se Fe[c] R (Å)	path Se Fe[c] σ^2 (Å²)
a	Se	6.0	7.5	3.2	1.68	0.002	1.8	3.35	0.004
b	Se	10.5	7.4	3.0	1.69	0.002	1.9	3.35	0.005
d	Se + Sr	10.5	7.0	3.2	1.69	0.003	1.8	3.35	0.005
e	Sr + Se	10.5	8.4	3.0	1.70	0.002	1.9	3.36	0.005
f	Se − Sr	10.5	7.5	3.1	1.69	0.003	1.9	3.37	0.007
g	Se + Sr	6.0	7.6	2.9	1.70	0.002	1.7	3.37	0.009

[a]Addition order is denoted with "+" and "−"; "+" represents stepwise addition and "−" represents simultaneous addition. [b]Amplitude reduction factor (S_0^2) = 0.90 for all models.[23,33] [c]The estimated errors: $N \pm 25\%$; $R \pm 0.02$ Å for the first shell and ± 0.05 Å for subsequent shells; $\sigma^2 \pm 25\%$.

Table 3. Best Fit EXAFS Model Parameters for Strontium Adsorbed on Goethite

coding	sample[a]	pH	ΔE_0 (eV)	N[b]	path Sr O[c] R (Å)	path Sr O[c] σ^2 (Å²)	path Sr O[c] N	path Sr O[c] R (Å)	path Sr O[c] σ^2 (Å²)
c	Sr	10.5	4.2	8.1	2.57	0.013	1.1	3.31	0.009
d	Se + Sr	10.5	3.7	7.3	2.56	0.012	1.4	3.36	0.006
e	Sr + Se	10.5	3.0	7.4	2.57	0.012	1.1	3.38	0.010
f	Se − Sr	10.5	4.7	7.4	2.55	0.012	1.5	3.24	0.018

[a]Addition order is denoted with "+" and "−"; "+" represents stepwise addition and "−" represents simultaneous addition. [b]Amplitude reduction factor (S_0^2) = 0.92 for all models.[32] [c]The estimated errors: $N \pm 25\%$; $R \pm 0.02$ Å for the first shell and ± 0.05 Å for subsequent shells; $\sigma^2 \pm 25\%$.

In a next step, the coadsorption of selenite and various cations is studied by electrokinetic measurements. Results are presented in the SI Figure S2. Similarities between Sr(II) and Ca(II) on the one hand side and monovalent cations on the other hand side are obvious. Overall, only the divalent cations are able to reverse the sign of electrophoretic mobility, which indicates specific binding of divalent cations at the particle surface. In contrast, adding monovalent cations caused a decrease of the absolute electrophoretic mobility, but no inversion of the sign from negative to positive, indicate mere screening instead of specific binding adsorption. In the ternary system, a similar trend but with decreased overall electro phoretic mobility is observed.

The addition order of cations and anions is also examined. Results (SI Figure S3) show no more than minor differences in electrophoretic mobility, suggesting that the addition order has no influence on ion adsorption.

3.2. Solute Uptake. Batch adsorption experiments are carried out to quantify solute uptake. As shown in Figure 2A, Sr(II) and Se(IV) show classic cationic and anionic adsorption trends versus pH, consistent with previous studies.[19,26] In detail, in the cation binary system, Sr(II) adsorption gradually increases with increasing pH, reaches 10% at pH 9.5, and shows a sharp increase at pH > 10.5. Se(IV) adsorption gradually increases with decreasing pH up to 90% at pH 5. The adsorption of Sr(II) and Se(IV) in the ternary system is mutually and significantly enhanced. This effect is most pronounced in the respective pH regions of low adsorption. The enhancement of uptake is more significant for Sr(II) than for Se(IV) under environmentally relevant pH conditions. For example, within the typical groundwater pH range 6−8, the adsorption of Sr(II) increases by an average factor of 5, while the fractional adsorption of Se(IV) increases by less than 10%. The solute uptake data are well described by the simple (cf. SI Figure S5 and Table S1) and the full CD MUSIC model (cf. section 3.4).

Electrokinetic data are also recorded for the batch sorption samples. As before (Figure 1), the IEP shifts toward lower values upon addition of Se(IV) (Figure 2B), which confirms the strong ability of Se(IV) to alter the protonation behavior of the surface functional groups. This is a strong indication for an inner sphere interaction. Sr(II) adsorption increases the IEP in the binary system.

3.3. EXAFS. EXAFS measurements are conducted to explore the molecular structures of surface species and the possible influence of addition order. Within adsorption samples, good reproducibility is observed from comparison of XANES or EXAFS spectra (SI Figure S4). The unchanged position of the absorption edge indicates no valence state variation of selenium. The very similar spectral features in the post edge region suggest that there are no significant differences in the coordination environments as a function of pH or as an effect of the mutual presence of Se(IV) or Sr(II).

The EXAFS spectra are uniformly background subtracted, and spectra of binary and ternary adsorption samples are carefully compared to determine the presence or absence of extra backscatterers. Best fit structures ("S", "D", and "T" denote singly, doubly, and triply coordinated hydroxyl groups at the goethite surface, respectively) and corresponding model calculations are shown in Figure 3. The model parameters are summarized in Tables 2 and 3.

For selenium, two shells of backscattering atoms may be identified at $R + \Delta \sim 1.5$ and ~ 3.0 Å in all Fourier transform spectra (FTs) shown in Figure 3A. These contributions are modeled satisfactorily with an O shell at 1.69 ± 0.02 Å, containing 3.1 ± 0.3 atoms, and an Fe shell at 3.36 ± 0.02 Å, containing 1.8 ± 0.5 atoms, in good agreement with previous EXAFS analysis of Se(IV) adsorption on goethite.[23] The bidentate binuclear (corner sharing) binding fashion of Se(IV) and the inner sphere complexation are confirmed based on the best fit parameters and the geometrical information about the (110) face. There is no significant difference between samples prepared at pH 10.5 and samples prepared at pH 6, despite the differences in surface charge.

For strontium, the low surface loading at pH 6 leads to a high noise level and ambiguous details; the data for this sample are not shown. The other spectra are shown in Figure 3B, and the corresponding modeling results are summarized in Table 3.
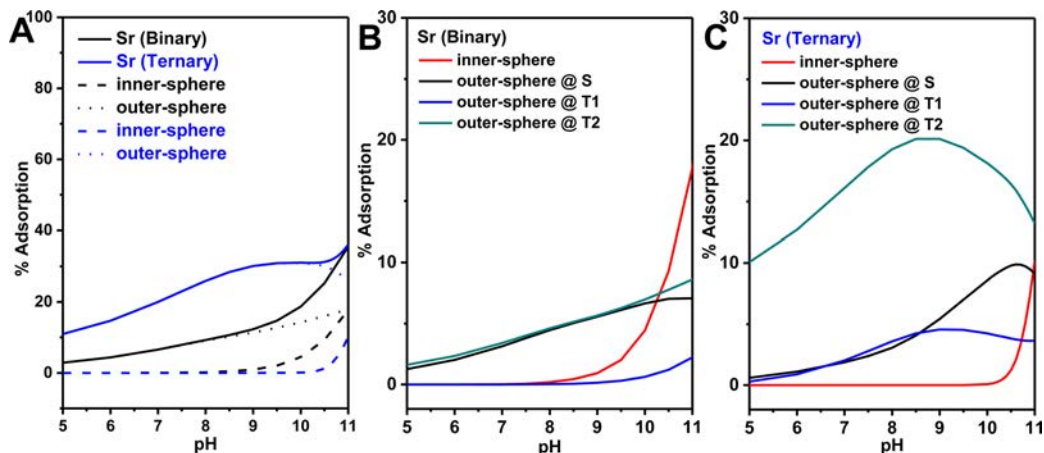
Figure 4. Species distribution of Sr surface complexes: (A) sums over inner and outer sphere complexes, (B) detailed speciation for the binary Sr–goethite system, and (C) species distribution in the ternary system (S, T1, and T2 denote Sr species binding with singly, triply I, and triply II coordinated hydroxyl group, respectively).

The FT peak is modeled with 7.6 ± 0.4 O atoms at 2.57 ± 0.02 Å, which is well reproducible and consistent with earlier EXAFS analysis of strontium adsorption on goethite.[25,26,32] The high Debye–Waller factors highlight the disorder of the coordination environment, probably including both hydration water molecules and surface hydroxyl groups. Axe et al.[36] examined the adsorption of Sr(II) on hydrous ferric oxide, and concluded that Sr(II) remains hydrated after adsorption. With respect to additional shells, we propose a second O shell with 1.2 ± 0.3 O at 3.3 ± 0.5 Å, which improves the model fit (reduces the R factor from 0.029 to 0.011). Two O shells could again be interpreted as O atoms from the coordinating water molecules and from surface hydroxyl groups. This might indicate a mixture of a small proportion of inner sphere with outer sphere Sr(II) surface complexes. More convincing evidence for Sr(II) inner sphere complexation on goethite surface can be found in previous studies.[24–26,32] Collins et al.[24] have modeled their spectra with 1.8 Fe at 4.3 Å, indicating Sr(II) adsorbed on goethite surface at pH 10.2 is inner sphere complex; Fuller et al.[25] have proposed two Fe shells (2.9 Fe atoms at 3.60 Å and 3.3 Fe atoms at 4.48 Å) for their adsorption sample at pH 12.6 and one Fe shell (3.5 Fe atoms at 3.56 Å) for the sample at pH 13.8. The adsorption structure that fits the geometrical constraints of Collins et al. is a bidentate binuclear inner sphere complex, involving two singly coordinated hydroxyl groups. A structure for Sr(II) binding at triply coordinated hydroxyl groups is deduced from Fuller et al. from the data indicating ~3 Fe neighbors at 3.6 Å.

Comparison between binary and ternary EXAFS samples does not indicate any direct interaction of Se(IV) and Sr(II) at the goethite surface. The absence of an effect of addition order points in the same direction and confirms the finding from electrokinetic investigations. For 0.25 mM adsorbates, the saturation of SrSeO₃ $(\log_{10}(K_{SP}) = -6.32^{37})$ is exceeded neither on the surface nor in solution. Furthermore, the data confirm the absence of carbonate contamination in our adsorption samples. Although Sr(II) and Se(IV) exhibit fast adsorption kinetics,[38,39] the adsorption of Se(IV) dominates over Sr(II) adsorption, whichever compound is added first (i.e., Se(IV) always forms an inner sphere surface complex and controls the overall surface potential). Finally, we may conclude from the EXAFS study that Se(IV) forms a bidentate inner sphere complex and that there are no ternary surface species, which is an important piece of information for the subsequent development of a surface complexation model.

3.4. CD-MUSIC Modeling. On the basis of the knowledge from batch experiments and EXAFS analysis, models are built to describe the surface reactions and explore the effect of coadsorption. The simplest model that fits both solute uptake and IEP data is listed in Table 1. Only one surface species for Se $[\equiv(FeO)_2SeO^-]$ is included in the model. Consistent with the EXAFS results, Se(IV) binds to two singly coordinated hydroxyl groups $(\equiv FeOH^{-1/2})$ and forms an inner sphere complex. The dominance of the bidentate species is also concluded by Hiemstra et al.,[19] while the addition of monodentate species does not significantly improve the modeling within our experimental conditions. For strontium, the presence of both outer sphere and inner sphere complexes would be in line with EXAFS results and literature data.[24,25] In this model, Cl⁻ binding with Sr surface species is included to allow the modeling of electrokinetic data (i.e., IEPs). In a similar fashion, Hiemstra[21] introduced Na⁺ adsorption to phosphate surface species. The dependency of Sr(II) adsorption on salt concentration is not studied in this work. The distinction between inner sphere and outer sphere adsorption is made by placing charge in different layers in the three plane model as indicated by the Δz parameters shown in Table 1.

Overall, the model describes the adsorption data (Figure 2A) satisfactorily, except the slight underestimation for Sr(II) ternary adsorption at pH < 7.5. The surface speciation of Se(IV) is represented by the bidentate binuclear species $[\equiv(FeO)_2SeO^-]$. Concerning Sr(II), as Figure 4A shows, the dominant species within pH 5–11 is an outer sphere complex, and the dominance is enhanced in the presence of Se(IV). The influences of Se(IV) on the Sr(II) surface complexes are as follows: the presence of Se(IV) inhibits the formation of the Sr(II) inner sphere complex due to competition effects, but it promotes the formation of outer sphere complexes due to electrostatic effects. These separate effects become clearer in Figures 4B and 4C: outer sphere complexation increases significantly in the ternary system, while both inner sphere and outer sphere binding with singly coordinated surface groups is limited by competition at pH < 9. On the basis of EXAFS and electrophoretic mobility results in combination with the modeling results, it is safe to conclude that the

electrostatic interaction dominates the coadsorption of Sr(II) and Se(IV) on goethite, explaining the mutual enhancement of adsorption.

With respect to modeling electrokinetic data, our model satisfactorily reproduces experimental IEP values of pure goethite, binary and ternary samples (Figure 1 and 2B). Considering a constant factor between the electrophoretic mobility and calculated diffuse layer potential, our model also predicts the corresponding pH trends satisfactorily (Figure 2B). Various complexities of modeling are reported in the literature.[12,21] Although additional tests are conducted (details are given in the SI), certainly we cannot cover all potential combinations of parameters. We can only assert that the model in Table 1 is the best model we tested. Note that a simpler model (SI Table S1) was developed initially during the optimization process. This model reproduces the adsorption data well, but fails to reproduce the IEP values (SI Figure S5). Comparison between the simple and full models indicates that the reason for this lapse lies in the oversimplification of the surface. The particle charge is an overall property involving all surface sites on all crystal faces, while adsorption typically happens on specific sites. Thus, the inclusion of an extra triply coordinated surface group with higher site density and of chloride complexes in the full model results in a better description of electrokinetic information, while it is not necessary to quantify adsorption.

4. ENVIRONMENTAL IMPLICATIONS

The fate of Se(IV) and Sr(II) in surface or subsurface environments is of concern, particularly with respect to the safe disposal of radioactive wastes and the fate of contaminated sites. For a comprehensive understanding of their migration or geochemical immobilization behaviors, studies addressing not only the binary systems, but tackling the challenges of the ternary and more complicated mixed system, are needed. Furthermore, it is crucial to explore the mechanism of the potential interactions on the molecular scale.

Se(IV) forms an inner sphere complex at goethite surfaces within the whole pH range, while Sr(II) forms outer sphere complexes at low and intermediate pH and inner sphere complexes at elevated pH. The presence of Se(IV) in the ternary system promotes the formation of the Sr(II) outer sphere complexes but inhibits the formation of Sr(II) inner sphere complexes. A mutual enhancement of adsorption driven by electrostatic interactions is observed between divalent cations (Sr(II) and Ca(II)) and Se(IV). Our result suggests that the synergistic effect significantly affects Sr(II) and Se(IV) uptake in the natural water pH range. For example, in the presence of 0.25 mM Se(IV), the overall adsorption of Sr(II) is promoted by an average factor of 5 at pH 6−8. Yet, the synergistic effect may be limited in cases where the surface loading is too low to significantly alter surface charge, but assuming a similar enhancement of Sr(II) adsorption in the presence of naturally abundant carbonate, this effect may be highly relevant in natural systems.

Models are established to predict complex systems based on the thermodynamics derived from simple systems. However, it is worthwhile to note the limitation of one specific model. During model development in this study, the direct combination of two binary models did not reproduce the ternary data, even in the absence of direct ternary chemical interaction. Moreover, one initially developed model can reproduce the adsorption data well, fails to reproduce all IEP values. Considering that, in general, researchers need to keep their models as simple as possible to satisfactorily reproduce specific data sets, our study demonstrates once more that the possibility to apply such models to more complex systems without further constraints is limited.

AUTHOR INFORMATION

Corresponding Authors
*E mail: frank.Heberling@kit.edu.
*E mail: liucl@pku.edu.cn.

ORCID ⊙
Frank Heberling: 0000 0002 2650 2071
Tim Pruessmann: 0000 0002 7903 9199
Chunli Liu: 0000 0003 1400 3758

Notes
The authors declare no competing financial interest.

REFERENCES

(1) Brookins, D. G. *Geochemical Aspects of Radioactive Waste Disposal*; Springler Verlag: New York, USA, 1984.

(2) Toulhoat, P. Confinement and migration of radionuclides in a nuclear waste deep repository. *C. R. Phys.* 2002, 3 (7), 975−986.

(3) Ishihara, Y.; Ishiguro, K.; Umeki, H. *Effect of Change in Half Life of SE 79 on the Safety of HLW Geological Disposal System*; JNC TN8400 99 086; Japan Nuclear Cycle Development Institute: Japan, 1999.

(4) Casacuberta, N.; Masque, P.; Garcia Orellana, J.; Garcia Tenorio, R.; Buesseler, K. O. [90]Sr and ^{89}Sr in seawater off Japan as a consequence of the Fukushima Dai ichi nuclear accident. *Biogeosciences* 2013, 10 (6), 3649−3659.

(5) Holben, D. H.; Smith, A. M. The diverse role of selenium within selenoproteins: a review. *J. Am. Diet. Assoc.* 1999, 99 (7), 836−843.

(6) Romanyukha, A. A.; Ignatiev, E. A.; Degteva, M. O.; Kozheurov, V. P.; Wieser, A.; Jacob, P. Radiation doses from Ural region. *Nature* 1996, 381 (6579), 199−200.

(7) Rovira, M.; de Pablo, J.; El Armani, S.; Duro, L.; Grive, M.; Bruno, J. *Study of the Role of Magnetite in the Immobilization by Reduction to U (VI) under the Presence of H_2 (g) in Hydrogen Carbonate Medium*; SKB Technical Report TR 03 04; Swedish Nuclear Fuel and Waste Management Co (SKB): Stockholm, Sweden, 2003.

(8) Zhang, W. X. Nanoscale iron particles for environmental remediation: an overview. *J. Nanopart. Res.* 2003, 5 (3−4), 323−332.

(9) Kinniburgh, D. G.; Jackson, M. L.; Syers, J. K. Adsorption of alkaline earth, transition, and heavy metal cations by hydrous oxide gels of iron and aluminum. *Soil Sci. Soc. Am. J.* **1976**, *40* (5), 796−799.

(10) Cornell, R. M.; Schwertmann, U. *The Iron Oxides: Structure, Properties, Reactions, Occurrences and Uses*; Wiley VCH: Weinheim, Germany, 2003.

(11) Weidler, P. G.; Schwinn, T.; Gaub, H. G. Vicinal faces on synthetic goethite observed by atomic force microscopy. *Clays Clay Miner.* **1996**, *44* (4), 437−442.

(12) Hiemstra, T.; Venema, P.; Van Riemsdijk, W. H. Intrinsic proton affinity of reactive surface groups of metal (hydr)oxides: The bond valence principle. *J. Colloid Interface Sci.* **1996**, *184* (2), 680−692.

(13) Hiemstra, T.; Van Riemsdijk, W. H. A surface structural approach to ion adsorption: the charge distribution (CD) model. *J. Colloid Interface Sci.* **1996**, *179* (2), 488−508.

(14) Lützenkirchen, J.; Boily, J. F.; Lövgren, L.; Sjöberg, S. Limitations of the potentiometric titration technique in determining the proton active site density of goethite surfaces. *Geochim. Cosmochim. Acta* **2002**, *66* (19), 3389−3396.

(15) Boily, J. F.; Lützenkirchen, J.; Balmès, O.; Beattie, J.; Sjöberg, S. Modeling proton binding at the goethite (α FeOOH)−water interface. *Colloids Surf., A* **2001**, *179* (1), 11−27.

(16) Hiemstra, T.; Van Riemsdijk, W. H. A surface structural model for ferrihydrite I: Sites related to primary charge, molar mass, and mass density. *Geochim. Cosmochim. Acta* **2009**, *73* (15), 4423−4436.

(17) Parfitt, R. L.; Russell, J. D. Adsorption on hydrous oxides. IV. Mechanisms of adsorption of various ions on goethite. *J. Soil Sci.* **1977**, *28* (2), 297−305.

(18) Xie, J.; Gu, X.; Tong, F.; Zhao, Y.; Tan, Y. Surface complexation modeling of Cr (VI) adsorption at the goethite−water interface. *J. Colloid Interface Sci.* **2015**, *455*, 55−62.

(19) Hiemstra, T.; Rietra, R. P.; Van Riemsdijk, W. H. Surface complexation of selenite on goethite: MO/DFT geometry and charge distribution. *Croat. Chem. Acta.* **2007**, *80* (3−4), 313−324.

(20) Gaboriaud, F.; Ehrhardt, J. J. Effects of different crystal faces on the surface charge of colloidal goethite (α FeOOH) particles: an experimental and modeling study. *Geochim. Cosmochim. Acta* **2003**, *67* (5), 967−983. Stachowicz, M.; Hiemstra, T.; van Riemsdijk, W. H. Multi competitive interaction of As (III) and As (V) oxyanions with Ca^{2+}, Mg^{2+}, PO_3^{-4}, and CO_2^{-3} ions on goethite. *J. Colloid Interface Sci.* **2008**, *320* (2), 400−414.

(21) Rahnemaie, R.; Hiemstra, T.; van Riemsdijk, W. H. Geometry, charge distribution, and surface speciation of phosphate on goethite. *Langmuir* **2007**, *23* (7), 3680−3689.

(22) Tadanier, C. J.; Eick, M. J. Formulating the charge distribution multisite surface complexation model using FITEQL. *Soil Sci. Soc. Am. J.* **2002**, *66* (5), 1505−1517.

(23) Hayes, K. F.; Roe, A. L.; Brown, G. E., Jr.; Hodgson, K. O.; Leckie, J. O.; Parks, G. A. In situ X ray absorption study of surface complexes: Selenium oxyanions on goethite (α FeOOH). *Science* **1987**, *238*, 783−786.

(24) Collins, C. R.; Sherman, D. M.; Ragnarsdöttir, K. V. The adsorption mechanism of Sr2+ on the surface of goethite. *Radiochim. Acta* **1998**, *81* (4), 201−206.

(25) Fuller, A. J.; Shaw, S.; Peacock, C. L.; Trivedi, D.; Burke, I. T. EXAFS Study of Sr sorption to Illite, Goethite, Chlorite, and Mixed Sediment under Hyperalkaline Conditions. *Langmuir* **2016**, *32* (12), 2937−2946.

(26) Carroll, S. A.; Roberts, S. K.; Criscenti, L. J.; O'Day, P. A. Surface complexation model for strontium sorption to amorphous silica and goethite. *Geochem. Trans.* **2008**, *9*, 2.

(27) Bachmaf, S.; Planer Friedrich, B.; Merkel, B. J. Effect of sulfate, carbonate, and phosphate on the uranium (VI) sorption behavior onto bentonite. *Radiochim. Acta* **2008**, *96* (6), 359−366.

(28) Guo, Z.; Yan, C.; Xu, J.; Wu, W. Sorption of U (VI) and phosphate on γ alumina: binary and ternary sorption systems. *Colloids Surf., A* **2009**, *336* (1), 123−129.

(29) Zimina, A.; Dardenne, K.; Denecke, M. A.; Grunwaldt, J. D.; Huttel, E.; Lichtenberg, H.; Mangold, S.; Pruessmann, T.; Rothe, J.; Steininger, R.; Vitova, T. In The CAT ACT Beamline at ANKA: A new high energy X ray spectroscopy facility for CATalysis and ACTinide research. *J. Phys.: Conf. Ser.* **2016**, *712* (1), 012019.

(30) Ravel, B.; Newville, M. ATHENA, ARTEMIS, HEPHAESTUS: data analysis for X ray absorption spectroscopy using IFEFFIT. *J. Synchrotron Radiat.* **2005**, *12* (4), 537−541.

(31) Ankudinov, A. L.; Ravel, B.; Rehr, J. J.; Conradson, S. D. Real space multiple scattering calculation and interpretation of x ray absorption near edge structure. *Phys. Rev. B: Condens. Matter Mater. Phys.* **1998**, *58* (12), 7565−7576.

(32) Sahai, N.; Carroll, S. A.; Roberts, S.; O'Day, P. A. X ray absorption spectroscopy of strontium (II) coordination: II. Sorption and precipitation at kaolinite, amorphous silica, and goethite surfaces. *J. Colloid Interface Sci.* **2000**, *222* (2), 198−212.

(33) Peak, D. Adsorption mechanisms of selenium oxyanions at the aluminum oxide/water interface. *J. Colloid Interface Sci.* **2006**, *303* (2), 337−345.

(34) Westall, J. C. *FITEQL: A Computer Program for Determination of Chemical Equilibrium Constants from Experimental Data*; Department of Chemistry, Oregon State University: Corvallis, OR, USA, 1982.

(35) Poeter, E. P.; Hill, M. C. *Documentation of UCODE: A Computer Code for Universal Inverse Modeling*; DIANE Publishing: Denver, CO, USA, 1998.

(36) Axe, L.; Bunker, G. B.; Anderson, P. R.; Tyson, T. A. An XAFS analysis of strontium at the hydrous ferric oxide surface. *J. Colloid Interface Sci.* **1998**, *199* (1), 44−52.

(37) Olin, Å.; Noläng, B.; Öhman, L. O.; Osadchii, E. G.; Rosén, E. *Chemical Thermodynamics of Selenium*; North Holland Elsevier Science Publishers B. V.: Amsterdam, The Netherlands, 2005.

(38) Jang, M.; Pak, S.; Kim, M. J. Comparison of adsorption characteristics of Se (IV) and Se (VI) onto hematite: effects of reaction time, initial concentration, pH, and ionic strength. *Environ. Earth Sci.* **2015**, *74* (2), 1169−1173.

(39) Axe, L.; Anderson, P. R. Sr diffusion and reaction within Fe oxides: Evaluation of the rate limiting mechanism for sorption. *J. Colloid Interface Sci.* **1995**, *175* (1), 157−165.